THE JOURNAL OF PHYSICAL CHEMISTRY C

Article

pubs.acs.org/JPCC

Impact of Local Curvature and Structural Defects on Graphene–C_{60} Fullerene Fusion Reaction Barriers

Bartosz Trzaskowski,[†,‡] Ludwik Adamowicz,*[,†] Warren Beck,[§] Krishna Muralidharan,[∥] and Pierre A. Deymier[∥]

[†]Department of Chemistry, University of Arizona, Tucson, Arizona 85721, United States

[‡]Centre of New Technologies (CeNT), University of Warsaw, 02-089 Warszawa, Poland

[§]Department of Physics, University of Arizona, Tucson, Arizona 85721, United States

[∥]Department of Materials Science and Engineering, University of Arizona, Tucson, Arizona 85721, United States

Supporting Information

ABSTRACT: Self-consistent charge density functional tight-binding and density functional theory calculations have been employed to study the energetics of the graphene–C_{60} fullerene fusion. We show that there is an optimal value of the bond-puckering angle of single-layer graphene-like systems, which facilitates fusion with other low-dimension carbon systems. Specifically, chemical attachment of a C_{60} fullerene to a single-layer graphene sheet is not feasible from the energetic point of view due to lack of puckering of the pristine graphene surface, but may occur for systems with some surface curvature. The presence of various defects in the graphene surface, including formation of four- and five-membered rings, Stone–Wales defects, or single and double vacancies may create some surface strain leading to formation of reactive sites in graphene, which are susceptive to binding with a fullerene. As an example, we show that a single vacancy in the graphene surface can lead to formation of a stable chemical bond with a fullerene.

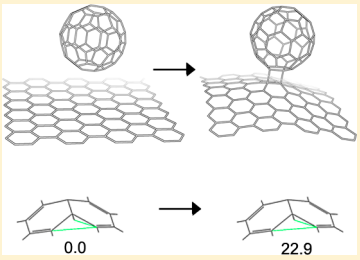

INTRODUCTION

Graphene is one of the most promising technological materials due to its outstanding electronic, mechanical, and thermal properties.[1−6] In recent years, it has been realized that hybrid materials composed of graphene and other low-dimension sp^2 carbon systems, like nanotubes and fullerenes, may add to this remarkable array of properties. For example, carbon nanotube peapods, fullerenes inside carbon nanotubes (CNTs)[7−9] and nanobuds, fullerenes attached to either the outer surface of single-walled carbon nanotubes (SWCNTs)[10−12] or graphene, have been suggested as building blocks of nanoelectronic devices and have promise in the field of spintronics.[13,14] The later may also serve as a precursor to the synthesis of pillared graphene structures, which are predicted to have remarkable structural, thermal, and electronic transport properties.[15−18] To date, however, graphene–fullerene peapod structures have yet to be synthesized experimentally and only recently a first step toward controlled synthesis of pillared graphene has been made.[19]

Experimental synthesis of a graphene–fullerene system may appear feasible, based on its similarity to a fullerene–fullerene system, for which experimental fusion has already been observed.[20−23] In the C_{60} dimer system, the energetically most favorable bond arrangement geometry involves two sigma bonds and formation of a four-membered square ring.[24] The energy barrier for the C_{60} dimer dissociation has been experimentally estimated to be between 1.25 and 1.56 eV.[25,26] However, a perfect graphene surface is known to be nonreactive (apart from its edges) due to its zero curvature.

From the chemical point of view , single-layer graphene (SLG) is a conjugated, chemically inert π-surface composed of aromatic sp^2-bonded carbon atoms. Carbon nanotubes, a similar sp^2-bonded carbon system, but with high curvature are, on the contrary, relatively reactive and can be functionalized rather easily.[27] The difference in reactivity of these two carbon systems is in part related to structural strain in nanotubes introduced by bending the planar SLG sheet, which causes curvature-induced pyramidalization at single carbon atoms[28] and π-orbital misalignment between adjacent pairs of carbon atoms.[29]

Various types of defects may help reduce activation energy barriers for fullerene attachment to SLG, either by acting as nucleation centers for chemical functionalization of graphene[30,31] or by introducing high lattice strain centers via forcing local curvature of the graphene structure. While graphene is known for the high formation energies of point defects resulting in low defects concentration,[32] point defects do exist in graphene[33−35] and can be deliberately introduced using various methods, like irradiation or chemical or mechanical treatment.[36−38]

Received: May 29, 2013
Revised: August 26, 2013
Published: August 29, 2013

In this work we use the self-consistent charge density functional tight-binding (SCC-DFTB) and density functional theory (DFT) methods to evaluate energy barriers for the formation of the SLG−C_{60} chemical bonding and provide critical information in relation to the chemical synthesis of such systems. We explore the energetic profiles of the binding reaction (by calculating points along the reaction path) for pristine SLG sheets and evaluate the effect of various types of lattice defects on these profiles, including single and double vacancies and Stone−Wales defects. We also explore the effect of strain on the reactivity of graphene and compare it to the reactivity of carbon-nanocones, where high curvature is an intrinsic structural feature.[39] Finally, we also examine the performance of the DFTB method in describing carbon-based nanosystems. The present work sheds light on the energetic requirements related to the graphene−C_{60} fusion and provides some guidance for the experimentalists in synthesizing novel hybrid materials based on graphene and fullerenes.

METHODS

The SCC-DFTB method (as implemented in DFTB+ software[40]) is used in the first part of this study. DFTB is a computational method based on a second-order expansion of the Kohn−Sham total energy in the density functional theory (DFT) with respect to charge density fluctuations.[41,42] The zeroth order approach in DFTB is equivalent to a common standard nonself-consistent tight-binding scheme, while at the second order a transparent, parameter-free, and readily calculable expression for generalized Hamiltonian matrix elements can be derived and used in determining the energy correction. These matrix elements are modified by a self-consistent redistribution of the Mulliken charges (SCC).[43] The DFTB method has been extensively used for modeling of carbon nanostructures, and the results were shown to be in good agreement with more sophisticated methods in the determination of equilibrium geometries, energies, and vibrational modes.[41,44−47]

In the present DFTB calculations, we use a periodic graphene sheet model containing 112 carbon atoms and a model of C_{60} fullerene for all modeled graphene systems (the models are shown in Figure 1). The models of various graphene defects including Stone−Wales defect,[48] single vacancy,[34] and double vacancy[49] are prepared based on a recent paper describing the most frequently occurring defects.[32] We also evaluate the energetics of the bonding between a fullerene and a carbon nanocone; here, a nanocone model is prepared based on a study of the nanocone reactivity.[50] In the optimization of all structures, they have been relaxed until atomic forces fall below 0.3 meV. A Monkhorst−Pack 3 × 3 × 3 point mesh is used for the periodic systems in the calculations.[51] Dispersion interactions are included via a Lennard-Jones potential between each pair of atoms with the parameters taken from the Universal Force Field.[52]

In the second part of the investigation we use the M06-2X DFT method[53] as implemented in the Gaussian09 software.[54] We use the 6-31+G* (for smaller systems) or 3-21G* (for larger systems) basis sets for geometry optimizations. To perform single-point calculations, we use the 6-31G* or 6-31+G* basis sets. Because of the computational limitations, we also used the ONIOM method[55] for single-point calculations with the atoms close to the bond-formation region described at the M06-2X/6-31+G* level and other atoms described at the M06-2X/3-21G* (denoted as ONIOM1 in the text) or PM6[56] (denoted as ONIOM2 in the text) levels. Throughout the text, we use the notation method1//method2, which means that the geometry of a particular system is optimized at the method1 level and then a single-point energy calculation is performed at the more accurate method2 level. In all DFT calculations involving graphene we use a graphene flake consisting of 168 carbon atoms and terminated with hydrogen atoms (without periodic boundary conditions). The defects in this graphene model are prepared in the same way as in the DFTB calculations. For structure optimization, we use the standard Gaussian convergence criteria with the SCF = tight keyword.

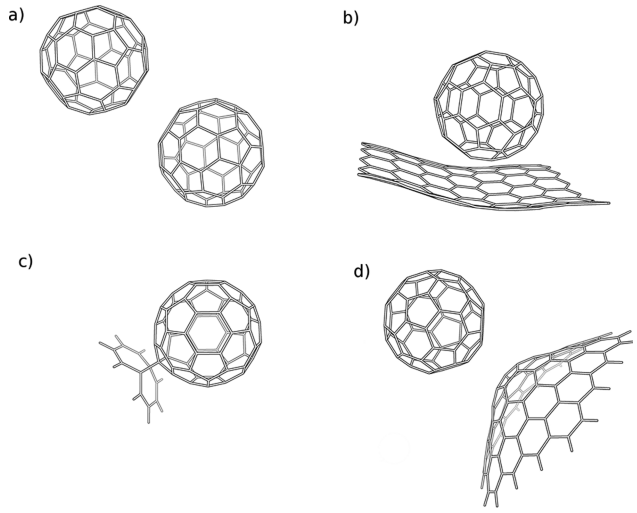

Figure 1. Molecular systems used in this study: (a) C_{60}−C_{60} model, (b) C_{60}−graphene model, (c) C_{60}−naphthalene model, and (d) C_{60}−nanocone model.

RESULTS

C_{60}−C_{60} Systems versus C_{60} Fullerene Interacting with Nondefective Graphene Surface. To better understand the fullerene−SLG systems and to validate the computational methods used in this work, we first estimate the dissociation energy barrier in the C_{60} dimer using an approach similar to the one used in the older study.[44] In that work, the authors looked at two different bond dissociation paths of the C_{60} fullerene dimer. In the first path (path-1), both C−C bonds connecting the two fullerenes are fixed by freezing the coordinates of the four carbon atoms participating in their formation. The remaining atoms are free to relax in the energy minimization. In the second path (path-2), only the carbon atoms forming one of the two C−C bonds connecting the two fullerenes are frozen; this approach is more realistic. We also include a third path where two C_{60} fullerenes interact via π−π stacking (path-3). The energy minimum in this path corresponds to the fullerenes being 3.56 Å apart (path-3).

We first consider calculations of the energy barriers for the C_{60}−C_{60} bond formation/dissociation using SCC-DFTB and DFT. The activation energy for the bond dissociation for path-1 is equal to 1.88 eV with the transition state located at the C−C bond distance of about 2.19 Å. The activation energy along path-2 (a more realistic approach) is equal to 1.05 eV at the C−C bond distance of 2.29 Å (the DFTB result; see Figure 2). The second value should be considered as a lower limit of the energy barrier, and it is in good agreement with the experimental estimate. It is also closer to the semiempirical AM1 value of 1.85 eV obtained in an older study.[57] It is worth

dx.doi.org/10.1021/jp405301e | J. Phys. Chem. C 2013, 117, 19664−19671

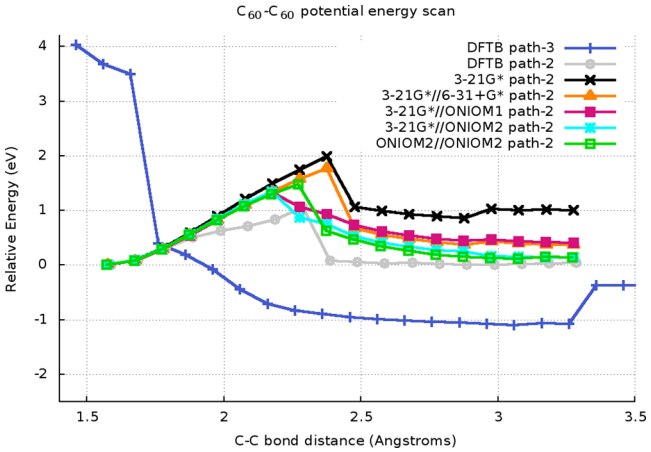

Figure 2. C_{60}−C_{60} potential energy surface (PES) along the reaction coordinate. No curve smoothing function has been used in the drawing of this and other PES profiles in this article. Instead, we decided to connect the calculated points with straight lines. As a result, the observed cusps have no physical origin such as singularities or conformational changes.

noting that the M06-2X/3-21G* method overestimates this energy barrier giving the value of 1.98 eV. The 3-21G*// 6-31+G* curve (using geometry optimized with the 3-21G* basis set) gives the energy barrier of 1.77 eV, while both ONIOM approaches give the value of 1.47 eV, in perfect agreement with the experimental data. Because of the good agreement with the experimental results, further calculations are performed only with the DFTB and 3-21G*//ONIOM2 methods. These methods combine good computational speed with good accuracy.

Next, we consider a C_{60} interacting with SLG (Figures 3a,b) using the DFTB method (DFT gives identical results). The interaction in this structure originates from the relatively weak π−π stacking of the adjacent benzene rings of the fullerene and

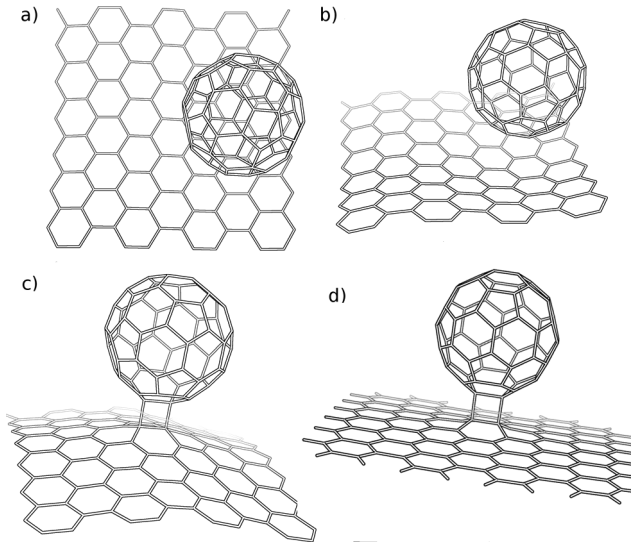

Figure 3. Models for C_{60} fullerene interacting with a graphene sheet: (a) interaction via π−π stacking, top view; (b) interaction via π−π stacking, side view; (c) C_{60} fullerene chemically bonded to SLG optimized at the DFTB level of theory; (d) C_{60} fullerene chemically bonded to SLG optimized at the DFT level of theory.

graphene. The equilibrium C−C distance is 3.0 Å, in agreement with both the experimental and theoretical data.[58,59]

A C_{60} fullerene chemically bound to a pristine SLG can be obtained in an analogous way to the fullerene dimer, utilizing a [2 + 2] cycloaddition reaction. Both DFTB and DFT methods show that such a system should be stable or at least metastable. In this system, the newly formed two σ C−C bonds have the lengths of 1.62 (DFTB) or 1.61 Å (DFT), which is slightly more than for the corresponding distances in the C_{60} dimer. It is interesting to note that in this system the graphene sheet exhibits a noticeable local curvature at the site of the new bond, which is identical for both DFTB-optimized and DFT-optimized structures (Figure 3c,d).

Figure 4 depicts the energy scan along a possible reaction coordinate of the C_{60} fullerene−SLG fusion obtained using

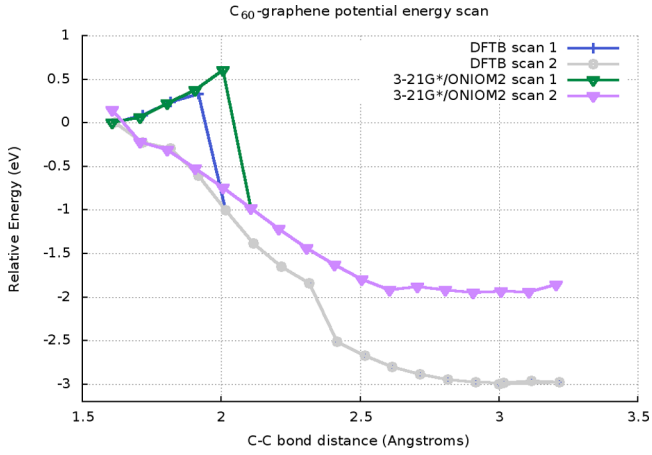

Figure 4. C_{60}−SLG potential energy surface along the reaction coordinate.

DFTB and DFT methods. At each point of the scan the distances between the carbon atoms of fullerene and graphene are changed in increments of 0.1 Å and all other degrees of freedom are free to relax. An energy scan (scan-1) along one of the σ C−C bonds, which is a possible reaction coordinate of C_{60} fullerene−SLG dissociation/fusion when starting from this structure of the adduct, reveals a 0.33 eV (DFTB) or 0.56 eV (DFT) energy barrier for the fullerene−SLG dissociation. However, a scan in the other direction (bond formation) starting from a nonbonded system (scan-2) shows that no chemical bonding occurs even at close distances. These results suggest that the spontaneous formation of a chemical bond between C_{60} fullerene and SLG is very unlikely since it requires following a very specific reaction path with a large energy barrier (3.3 eV) for bond formation and a low energy barrier for bond dissociation.

Next we evaluate whether curvature in the C_{60} dimer system distinguishes bonding in this system from the lack of bonding in the C_{60}−SLG system. To understand the impact of the carbon system curvature on the binding energetics we have performed additional calculations using a system of C_{60} fullerene interacting with naphthalene as a smaller SLG molecule analogue, but where development of some curvature during bonding is permitted (Figures 5a−c). For this and other systems, we examine the bond-puckering angle defined in Figure 5d. The optimized C_{60}−naphthalene bonded system is very similar to the C_{60}−C_{60} dimer system with the C−C distance of 1.60 Å. The bond-puckering angle of the bonded

dx.doi.org/10.1021/jp405301e | J. Phys. Chem. C 2013, 117, 19664−19671

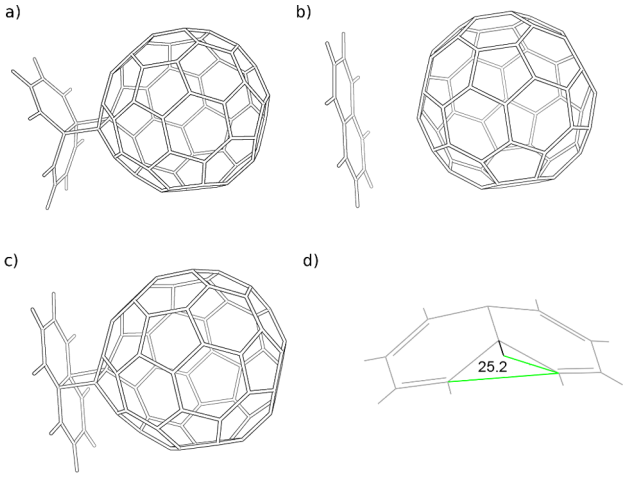

Figure 5. C_{60}–naphthalene system: (a) minimum-energy structure of bonded system; (b) minimum-energy structure of interacting system; (c) model of a C_{60} fullerene bonded to a flat naphthalene; (d) definition of the bond-puckering angle.

naphthalene molecule is 25.2°, while the bond-puckering angle of the adjacent fullerene bonds interacting with the naphthalene is 30.9°. For comparison, the bond angle of an isolated fullerene is 20.9° (DFTB) or 21.1° (DFT), whereas the bond angles of the comparable adjacent bonds in the bonded C_{60} dimer system is 30.6° (DFTB) or 30.7° (DFT). The C_{60}–naphthalene system resembles the C_{60} dimer system as the potential energy scan along the C–C bond are both very similar, each with a dissociation energy barrier of 1.20 eV on the DFTB level.

Preventing the naphthalene bond angle from rotating (by freezing certain carbon atoms in the course of computations) has a drastic effect on the energetics of the reaction (Figure 6). If we consider a zero degree bond angle (as in ideal, noninteracting SLG), we obtain a completely different potential energy curve with a very high energy barrier and a low binding energy due to unfavorable overlap of π orbitals. A bond-puckering angle of 22.9° (as in graphene interacting with C_{60} fullerene, see Figure 4) gives a similar barrier to the relaxed

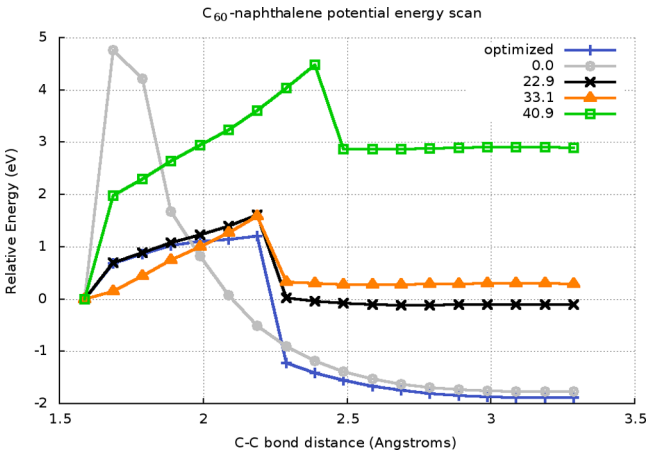

Figure 6. C_{60}–naphthalene potential energy surfaces along the reaction coordinate (DFTB level). Different values correspond to the different bond-puckering angles, which were frozen during the scan. Optimized curve corresponds to the potential energy scan where the bond-puckering angle was being optimized at each step of the potential energy scan.

system, but with a slightly higher energy barrier of 1.33 eV. Increasing the bond angle in the naphthalene molecule over the optimal angle of 30.9° also increases the energy barrier. For the bond-puckering angle of 33.1° we estimate the energy barrier to be 1.58 eV, while for 40.9° it is 2.69 eV. This data suggests that there is an optimal bond-puckering angle, equal to about 30.9°, which allows for the strongest bonding between these types of aromatic carbon–carbon systems.

Achieving this optimal bond angle, however, introduces an additional lattice strain energy term, which must be overcome so the resulting actual angle may differ somewhat from the optimal one. For C_{60} fullerene bonding to another C_{60} molecule there is only a relatively small bond angle rotation going from 20.9° (noninteracting C_{60} fullerene) to 30.6° (two C_{60} fullerenes forming a C_{120} system) required. Chemically attaching a fullerene to graphene, however, necessitates the bonds in the graphene sheet involved in the bonding to rotate from 0° to 22.9°. This requires overcoming a higher bond strain energy. We have evaluated the reorganization energy (defined as the energy required to change from the optimal angle of an noninteracting system to the optimal angle for the chemically bound system) at the M06-2X/3-21G* level of theory for both discussed systems. As expected, the reorganization energy for C_{60} fullerene is relatively low (1.42 eV), while for the SLG it is much higher and equal to 2.26 eV for a 0° to 22.9° change and 5.57 eV for a 0° to 30.9° change.

It is worth mentioning that similar studies concerning the impact of the curvature of nanosystems on their reactivity have been performed earlier for nanotubes.[60] In that work, a linear dependence between the CH_2/N/O exo and endo additions to armchair nanotubes and the inverse tube diameter is shown. The endo addition is relatively similar to the nanocones radical addition studied earlier, where a dependence between nanocone curvature and methylene radical addition was found. In our case, however, we observe no linear dependence between the reaction energy and curvature/bond-puckering angle. This is due to both the additional constraints caused by the overall geometry of C_{60} fullerene and the requirements of orbital overlap in the [2 + 2] cycloaddition reaction, resulting in one optimal curvature value.

These results suggest that chemical attachment of fullerenes to carbon structures with high intrinsic bond angle may have relatively low activation energy barriers. To test this hypothesis we evaluated potential energy curves for C_{60} interacting with a nanocone system with an intrinsic bond angle of 25.5° (Figure 1d). As expected, the potential energy scan for this system interacting with C_{60} fullerene is similar to the graphene–C_{60} case (Figure 7). The nanocone has a very similar barrier for the C–C bond dissociation of 0.8 eV due to a similar bond angle. It is not, however, as high as expected from a similar bond angle in the C_{60} fullerene–naphthalene system due to the presence of the four-membered aromatic ring, which is more reactive than the six-membered ring and additionally lowers the energy barrier.[50]

C_{60} Fullerene Interacting with Defective Graphene Surface. The second option for creating a more reactive graphene surface is to utilize naturally occurring surface defects, which may create highly reactive radicals and introduce nonzero curvatures on the SLG surface. To test this option, we have calculated potential energy surfaces for C_{60} fullerene interacting with the defect-containing SLG models presented in Figure 2. The calculations shows that in all considered cases the fullerene avoids the area where the defect is located, as it

dx.doi.org/10.1021/jp405301e | J. Phys. Chem. C 2013, 117, 19664–19671

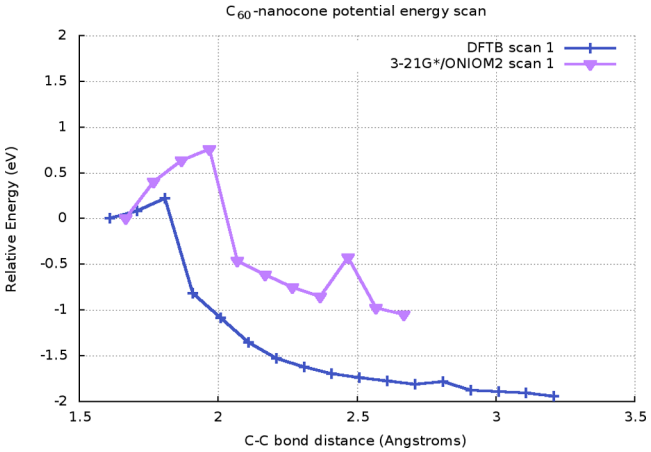

Figure 7. C_{60} nanocone potential energy surfaces along the reaction coordinate.

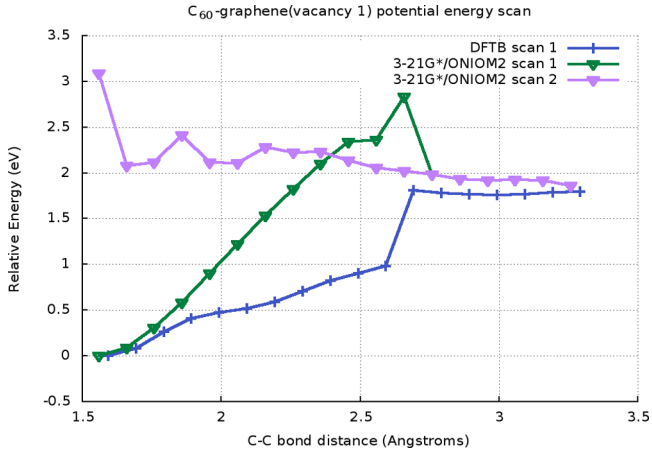

Figure 9. C_{60}–graphene (vacancy1) potential energy surface along the reaction coordinate.

distorts the $\pi-\pi$ stacking interaction between the adjacent surfaces of the graphene and C_{60} fullerene. The C–C distance between the fullerene and the graphene with a defect measured as the distance between the closest carbon atoms is in the range of 3.0–3.3 Å. The differences between interaction energies of the ideal and distorted $\pi-\pi$ stacking are, however, very small (on the order of 0.1 eV), and it is clear that even at the standard temperature the fullerene is able to move virtually freely around the whole surface of the defective graphene surface.

For C_{60} attachment to pristine SLG, we find only one minimum-energy configuration for chemical attachment, but it is thermodynamically unstable. For defected graphene sheets, however, there are, in some cases, multiple low energy configurations. For each investigated defect we have built multiple starting geometries, which have been subsequently used in the calculations. Here, we will only focus on the structures that are most energetically favorable (Figure 8).

For most of the studied cases, we found that the system behaves similarly to the C_{60}–C_{60} case, albeit with a much smaller energy barrier (see Supporting Information). Following the likely dissociation path of fullerene from the defected graphene sheet shows a small energy barrier; a scan in the direction of bond formation gives similar results. The height of the energy barrier is, however, in these cases around 0.5 eV, suggesting that the C_{60} fullerene is only weakly bound in these systems, and most likely no spontaneous formation of a chemical bond would be observed experimentally.

The lone exception is the single vacancy case (Figure 9b). In this case, the bonded system is highly asymmetric, forming strong carbon–carbon bonds (with bond distances of 1.56 and 1.59 Å, respectively). Breaking these bonds requires more than 2 eV suggesting that such bonding is very stable. This is also the only case in which we can see a true energy barrier for both the path of bond dissociation and the path of bond formation (see Figure 9).

CONCLUSIONS

In this work, we present a theoretical analysis of the first step involved in controlled C_{60} fullerene–graphene fusion, which, as we have suggested, could be a path toward synthesis of pillared graphene structures. Previous calculations for the C_{60}–C_{60} fullerene fusion indicate that it is a multistep, complex process with multiple metastable structures and complicated bond rearrangements.[61−63] The process is facilitated by creation of generalized Stone–Wales defects, which, due to the high strain they cause in fullerene molecules, lead to paths with relatively low activation-energy barriers to the C_{60}–C_{60} dimer formation. Conjoining C_{60} molecules via simultaneous formation of two new C–C sigma bonds is, however, the crucial step of the whole fusion process, despite its low activation barrier. As suggested earlier,[61] the [2 + 2] cycloaddition reaction may be a rate-limiting step for the fusion since it can be initiated only in a geometry of the system where two C–C bonds of the fullerenes face each other. There is a relatively low probability for thermal activation of cycloaddition, particularly at low temperatures, which may prevent fusion initiation. Han et al. estimated that this step should occur on the time scale of once a week per pair of C_{60} molecules at 1400 K, which is significantly longer than the time frame of a Stone–Wales transformation.[61] We note, however, that photochemical activation, where one component has an electron promoted to a pi-antibonding state, may

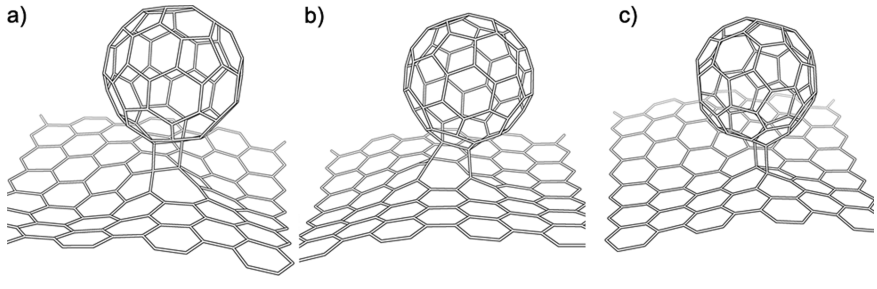

Figure 8. C_{60} fullerene attached to graphene sheet with various defects: (a) Stone–Wales defect; (b) single vacancy; (c) double vacancy 1.

dx.doi.org/10.1021/jp405301e | J. Phys. Chem. C 2013, 117, 19664–19671

significantly enhance cyclo-addition rates because of favorable orbital symmetry changes.[64]

We show that C_{60} fullerene bonding to SLG via thermal activation requires a similar, unlikely arrangement of C−C bonds and has a relatively high energy barrier. The dissociation of the new C−C bonds is, however, much more likely than in the C_{60} dimer case due to the presence of additional benzene rings in the graphene sheet, which may form favorable $\pi-\pi$ stacking interactions with the dissociating fullerene molecule, driving the reaction toward dissociation. Unlike the case of the C_{60} dimer, where the covalently bonded system is almost isoenergetic with the π-bonded system and the barrier from the former to latter is high, the C_{60}−graphene system is different. Here, the covalently bonded system is metastable by about 3 eV, and the barrier to go from the covalently bonded adduct to the significantly more stable, π-bonded complex is small. A barrier of this magnitude can be easily overcome by thermal activation. Therefore, we shall conclude that it would be highly unlikely to form a covalently bonded C_{60}−graphene system, and therefore, we would need either defect-mediation, attachment via chemical functionalization, or other means to achieve this.

However, we find that during fullerene bonding the graphene sheet's local curvature adjusts via local bond rotation/puckering in order to optimize the π orbitals overlap. We also show that there is an optimal C−C bond angle associated with this sheet curvature, which facilitates the attachment process. Carbon systems with intrinsic positive curvature (including fullerenes and carbon nanocones) possess lower energy barriers to fusion; whereas others (like graphene) are forced to distort their structure to facilitate the optimal bonding angle. This finding implies that graphene should become more reactive by artificially straining the graphene sheet. This could be accomplished by either introducing propagating dislocations,[65] by synthesizing single-sided hydrogenated graphene,[66] or via mechanical bending of the graphene sheet.[67] If such a deformation can be effectively achieved in a controlled manner, it may lead to a controlled fullerene−graphene fusion and synthesis of novel hybrid materials.

Introduction of defects in graphene is another method of distorting its structure, which may lead to lowering the activation energy barrier toward fusion with fullerenes. We show that the attachment of C_{60} fullerene to carbons at the edges of the defect is not more likely than the attachment to a pristine graphene sheet. This effect is due to the distortion of the ideal π system in graphene, which perturbs the $\pi-\pi$ stacking interaction with fullerene and forces fullerene to avoid the defective surface of graphene. However, a successful fullerene bonding creates in some cases a system with a shorter and stronger (harder to break) set of C−C bonds than in the case of graphene without defects. This behavior may be used, e.g., in a controlled synthetic process where a defect-containing graphene sheet is functionalized with fullerenes and subsequently heated to remove fullerenes attached to all carbon atoms but those involved in the defect.

We also show that the DFTB method is able to qualitatively reproduce the energetics of the C_{60} fullerene−graphene reactions. It has been shown earlier that this method is perfectly suited to describe and model graphene-based nanosystems (including the defects described in this work) at a fraction of the computational cost of the DFT methods.[68] In the case of the systems studied here, the difference in geometries of the DFTB-optimized and DFT-optimized systems is minor, although the reaction barriers differ to some extent, and in some cases substantially.

■ ASSOCIATED CONTENT

Supporting Information

Additional figures of C_{60} fullerene attached to graphene surface with various defects and graphs/tables with total energies of all modeled systems. This material is available free of charge via the Internet at http://pubs.acs.org.

■ AUTHOR INFORMATION

Corresponding Author

*(L.A.) Phone: +1 520 6216607. E-mail: ludwik@u.arizona.edu.

Author Contributions

The manuscript was written through contributions of all authors. All authors have given approval to the final version of the manuscript.

Notes

The authors declare no competing financial interest.

■ ACKNOWLEDGMENTS

We gratefully acknowledge support for this research from the United States National Science Foundation Division of Materials Research (award # 1148936) and the NSF Grants for Exploratory Research Program (EAGER). B.T. was partially supported by the "Mobilność Plus" program of the Ministry of Science and Higher Education of Poland.

■ REFERENCES

(1) Novoselov, K. S.; Geim, A. K.; Morozov, S. V.; Jiang, D.; Zhang, Y.; Dubonos, S. V.; Grigorieva, I. V.; Firsov, A. A. Electric Field Effect in Atomically Thin Carbon Films. *Science* **2004**, *306*, 666−669.

(2) Bae, S.; Kim, H.; Lee, Y.; Xu, X.; Park, J.-S.; Zheng, Y.; Balakrishnan, J.; Lei, T.; Kim, H. R.; Song, Y.; et al. Roll-to-Roll Production of 30-in. Graphene Films for Transparent Electrodes. *Nat. Nanotechnol.* **2010**, *5*, 574−578.

(3) Kim, K. S.; Zhao, Y.; Jang, H.; Lee, S. Y.; Kim, J. M.; Kim, K. S.; Ahn, J. H.; Kim, P.; Choi, J. Y.; Hong, B. H. Large-Scale Pattern Growth of Graphene Films for Stretchable Transparent Electrodes. *Nature* **2009**, *457*, 706−710.

(4) Berger, C.; Song, Z.; Li, T.; Li, X.; Ogbazghi, A. Y.; Dai, Z.; Marchenkov, A. N.; Conrad, E. H.; First, P. N.; de Heer, W. A. Ultrathin Epitaxial Graphite: 2D Electron Gas Properties and a Route toward Graphene-Based Nanoelectronics. *J. Phys. Chem. B* **2004**, *108*, 19912−19916.

(5) Berger, C.; Song, Z.; Li, X.; Wu, X.; Brown, N.; Naud, C.; Mayou, D.; Li, T.; Hass, J.; Marchenkov, A. N.; Conrad, E. H.; First, P. N.; de Heer, W. A. Electronic Confinement and Coherence in Patterned Epitaxial Graphene. *Science* **2006**, *312*, 1191−1196.

(6) Geim, A. K. Graphene: Status and Prospects. *Science* **2009**, *324*, 1530−1534.

(7) Smith, B. W.; Monthioux, M.; Luzzi, D. E. Encapsulated C_{60} in Carbon Nanotubes. *Nature* **1998**, *396*, 323−324.

(8) Smith, B. W.; Russo, R. M.; Chikkannanavar, S. B.; Luzzi, D. E. High-Yield Synthesis and One-Dimensional Structure of C_{60} Encapsulated in Single-Wall Carbon Nanotubes. *J. Appl. Phys.* **2002**, *91*, 9333−9340.

(9) Khlobystov, A. N.; Britz, D. A.; Ardavan, A.; Briggs, G. A. D. Observation of Ordered Phases of Fullerene in Carbon Nanotubes. *Phys. Rev. Lett.* **2004**, *92*, 245507.

(10) Nasibulin, A. G.; Pikhitsa, P. V.; Jiang, H.; Brown, D. P.; Krasheninnikov, A. V.; Anisimov, A. S.; Queipo, P.; Moisala, A.; Gonzalez, D.; Lientschnig, G.; et al. Novel Hybrid Carbon Material. *Nat. Nanotechnol.* **2007**, *2*, 156−161.

(11) Tian, Y.; Chassaing, D.; Nasibulin, A. G.; Ayala, P.; Jiang, H.; Anisimov, A. S.; Hassanien, A.; Kauppinen, E. I. The Local Study of a NanoBud Structure. *Phys. Status Solidi B* **2008**, *245*, 2047−2050.
(12) Tian, Y.; Chassaing, D.; Nasibulin, A. G.; Ayala, P.; Jiang, H.; Anisimov, A. S.; Kauppinen, E. I. Combined Raman Spectroscopy and Transmission Electron Microscopy Studies of a NanoBud Structure. *J. Am. Chem. Soc.* **2008**, *130*, 7188−7189.
(13) Wu, X. J.; Zeng, X. C. Periodic Graphene Nanobuds. *Nano Lett.* **2009**, *9*, 250−256.
(14) Wang, M.; Li, C. M. Magnetic Properties of All-Carbon Graphene-Fullerene Nanobuds. *Phys. Chem. Chem. Phys.* **2011**, *13*, 5945−5951.
(15) Dimitrakakis, G. K.; Tylianakis, E.; Froudakis, G. F. Pillared Graphene: A New 3-D Network Nanostructure for Enhanced Hydrogen Storage. *Nano Lett.* **2008**, *8*, 3166−3170.
(16) Tylianakis, E.; Psofogiannakis, G. M.; Froudakis, G. F. Li-Doped Pillared Graphene Oxide: A Graphene-Based Nanostructured Material for Hydrogen Storage. *J. Phys. Chem. Lett.* **2010**, *1*, 2459−2464.
(17) Varshney, V.; Patnaik, S. P.; Roy, A. K.; Froudakis, G.; Farmer, B. L. Modeling of Thermal Transport in Pillared-Graphene Architectures. *ACS Nano* **2010**, *4*, 1153−1161.
(18) Wesolowski, R. P.; Terzyk, A. P. Pillared Graphene As a Gas Separation Membrane. *Phys. Chem. Chem. Phys.* **2011**, *13*, 17027−17029.
(19) Du, F.; Yu, D.; Dai, L.; Ganguli, S.; Varshney, V.; Roy, A. K. Preparation of Tunable 3D Pillared Carbon Nanotube Graphene Networks for High-Performance Capacitance. *Chem. Mater.* **2011**, *23*, 4810−4816.
(20) Xu, C. H.; Scuseria, G. E. Theoretical Predictions for a Two-Dimensional Rhombohedral Phase of Solid C_{60}. *Phys. Rev. Lett.* **1995**, *74*, 274−277.
(21) Bajwa, N.; Ingale, A.; Avashti, D. K.; Kumar, R.; Dharamvir, K.; Jindal, V. K. Swift Heavy Ion Induced Modification Studies of C60 Thin Films. *J. Appl. Phys.* **2003**, *94*, 326−333.
(22) Bandow, S.; Takizawa, M.; Hirihara, K.; Yudasaka, M.; Iijima, S. Smallest Limit of Tube Diameters for Encasing of Particular Fullerenes Determined by Radial Breathing Mode Raman Scattering. *Chem. Phys. Lett.* **1991**, *337*, 48−54.
(23) Kim, Y. H.; Lee, I. H.; Chang, K. J.; Lee, S. Dynamics of Fullerene Coalescence. *Phys. Rev. Lett.* **2003**, *90*, 065501.
(24) Komatsu, K.; Wang, G.-W.; Murata, Y.; Tanaka, T.; Fujiwara, K.; Yamamoto, K.; Saunders, M. Mechanochemical Synthesis and Characterization of the Fullerene Dimer C_{120}. *J. Org. Chem.* **1998**, *63*, 9358−9366.
(25) Wang, Y.; Holden, J. M.; Bi, X.; Eklund, P. C. Thermal Decomposition of Polymeric C_{60}. *Chem. Phys. Lett.* **1994**, *217*, 413−417.
(26) Davydov, V. A.; Kashevarova, L. S.; Rakhmanina, A. V.; Senyavin, V. M.; Pronina, O. P.; Oleynikov, N. N.; Agafonov, V.; Ceolin, R.; Allouchi, H.; Szwarc, H. Pressure-Induced Dimerization of Fullerene C_{60}: a Kinetic Study. *Chem. Phys. Lett.* **2001**, *333*, 224−229.
(27) Hirsch, A. Functionalization of Single-Walled Carbon Nanotubes. *Angew. Chem., Int. Ed.* **2002**, *41*, 1853−1859.
(28) Chen, Z.; Thiel, W.; Hirsch, A. Reactivity of the Convex and Concave Surfaces of Single-Walled Carbon Nanotubes (SWCNTs) towards Addition Reactions: Dependence on the Carbon-Atom Pyramidalization. *ChemPhysChem* **2003**, *4*, 93−97.
(29) Hamon, M. A.; Itkis, M. E.; Niyogi, S.; Alvarez, T.; Kuper, C.; Menon, M.; Haddon, R. C. Effect of Rehybridization on the Electronic Structure of Single-Walled Carbon Nanotubes. *J. Am. Chem. Soc.* **2001**, *123*, 11292−11293.
(30) Nardelli, M. B.; Yakobson, B. I.; Bernholc, J. Mechanism of Strain Release in Carbon Nanotubes. *Phys. Rev. B* **1998**, *57*, R4277−R4280.
(31) OuYang, F.; Huang, B.; Li, Z.; Xiao, J.; Wang, H.; Xu, H. Chemical Functionalization of Graphene Nanoribbons by Carboxyl Groups on Stone-Wales Defects. *J. Phys. Chem. C* **2008**, *112*, 12003−12007.
(32) Banhart, F.; Kotakoski, J.; Krasheninnikov, A. V. Structural Defects in Graphene. *ACS Nano* **2011**, *5*, 26−41.
(33) Hashimoto, A.; Suenaga, K.; Gloter, A.; Urita, K.; Iijima, S. Direct Evidence for Atomic Defects in Graphene Layers. *Nature* **2004**, *430*, 870−873.
(34) Gass, M. H.; Bangert, U.; Bleloch, A. L.; Wang, P.; Nair, R. R.; Geim, A. K. Free-Standing Graphene at Atomic Resolution. *Nat. Nanotechnol.* **2008**, *3*, 676−681.
(35) Meyer, J. C.; Kisielowski, C.; Erni, R.; Rossell, M. D.; Crommie, M. F.; Zettl, A. Direct Imaging of Lattice Atoms and Topological Defects in Graphene Membranes. *Nano Lett.* **2008**, *8*, 3582−3586.
(36) Tapaszto, L.; Dobrik, G.; Nemes-Incze, P.; Vertesy, G.; Lambin, P.; Biro, L. P. Tuning the Electronic Structure of Graphene by Ion Irradiation. *Phys. Rev. B* **2008**, *78*, 233407.
(37) Coleman, V. A.; Knut, R.; Karis, O.; Grennberg, H.; Jansson, U.; Quinlan, R.; Holloway, B. C.; Sanyal, B.; Eriksson, O. Defect Formation in Graphene Nanosheets by Acid Treatment: an X-ray Absorption Spectroscopy and Density Functional Theory Study. *J. Phys. D: Appl. Phys.* **2009**, *41*, 062001.
(38) Compagnini, G.; Giannazzo, F.; Sonde, S.; Raineri, V.; Rimini, E. Ion Irradiation and Defect Formation in Single Layer Graphene. *Carbon* **2009**, *47*, 3201−3207.
(39) Jaszczak, J. A.; Robinson, G. W.; Dimovski, S.; Gogotsi, Y. Naturally Occurring Graphite Cones. *Carbon* **2003**, *41*, 2085−2092.
(40) Aradi, B.; Hourahine, B.; Frauenheim, T. DFTB+, a Sparse Matrix-Based Implementation of the DFTB Method. *J. Phys. Chem. A* **2007**, *111*, 5678−5684.
(41) Porezag, D.; Frauenheim, T.; Kohler, T.; Seifert, G.; Kaschner, R. Construction of Tight-Binding-Like Potentials on the Basis of Density-Functional Theory: Application to Carbon. *Phys. Rev. B* **1995**, *51*, 12947−12957.
(42) Seifert, G.; Porezag, D.; Frauenheim, T. Calculations of Molecules, Clusters, and Solids with a Simplified LCAO-DFT-LDA Scheme. *Int. J. Quantum Chem.* **1996**, *58*, 185−192.
(43) Elstner, M.; Porezag, D.; Jungnickel, G.; Elsner, J.; Haugk, M.; Frauenheim, T.; Suhai, S.; Seifert, G. Self-Consistent-Charge Density-Functional Tight-Binding Method for Simulations of Complex Materials Properties. *Phys. Rev. B* **1998**, *58*, 7260−7268.
(44) Porezag, D.; Pedersen, M. P.; Frauenheim, T.; Kohler, T. Structure, Stability, and Vibrational Properties of Polymerized C_{60}. *Phys. Rev. B* **1995**, *52*, 14963−14970.
(45) Irle, S.; Zheng, G.; Wang, Z.; Morokuma, K. The C_{60} Formation Puzzle "Solved": QM/MD Simulations Reveal the Shrinking Hot Giant Road of the Dynamic Fullerene Self-Assembly Mechanism. *J. Phys. Chem. B* **2006**, *110*, 14531−14545.
(46) Jakowski, J.; Irle, S.; Morokuma, K. Collision-Induced Fusion of Two C_{60} Fullerenes: Quantum Chemical Molecular Dynamics Simulations. *Phys. Rev. B* **2010**, *82*, 125443.
(47) Qian, H. J.; van Duin, A. C. T.; Morokuma, K.; Irle, S. Reactive Molecular Dynamics Simulation of Fullerene Combustion Synthesis: ReaxFF vs DFTB Potentials. *J. Chem. Theor. Comput.* **2011**, *7*, 2040−2048.
(48) Stone, A. J.; Wales, D. J. Theoretical Studies of Icosahedral C_{60} and Some Related Species. *Chem. Phys. Lett.* **1986**, *128*, 501−503.
(49) Krasheninnikov, A. V.; Lehtinen, P. O.; Foster, A. S.; Nieminen, R. M. Bending the Rules: Contrasting Vacancy Energetics and Migration in Graphite and Carbon Nanotubes. *Chem. Phys. Lett.* **2006**, *418*, 132−136.
(50) Trzaskowski, B.; Jalbout, A. F.; Adamowicz, L. Functionalization of Carbon Nanocones by Free Radicals: A Theoretical Study. *Chem. Phys. Lett.* **2007**, *444*, 314−318.
(51) Monkhorst, H. J.; Pack, J. D. Special Points for Brillouin-Zone Integrations. *Phys. Rev. B* **1976**, *13*, 5188−5192.
(52) Rappe, A. K.; Casewit, C. J.; Colwell, K. S.; Goddard, W. A.; Skiff, W. M. UFF, a Full Periodic Table Force Field for Molecular Mechanics and Molecular Dynamics Simulations. *J. Am. Chem. Soc.* **1992**, *114*, 10024−10035.
(53) Zhao, Y.; Truhlar, D. G. The M06 Suite of Density Functionals for Main Group Thermochemistry, Thermochemical Kinetics, Non-

covalent Interactions, Eexcited States, and Transition Elements: Two New Functionals and Systematic Testing of Four M06-Class Functionals and 12 Other Functionals. *Theor. Chem. Acc.* **2008**, *120*, 215−241.
(54) Frisch, M. J.; Trucks, G. W.; Schlegel, H. B.; Scuseria, G. E.; Robb, M. A.; Cheeseman, J. R.; Scalmani, G.; Barone, V.; Mennucci, B.; Petersson, G. A.; et al. *Gaussian 09*, revision A.1; Gaussian, Inc.: Wallingford, CT, 2009.
(55) Dapprich, S.; Komaromi, I.; Byun, K. S.; Morokuma, K. A New ONIOM Implementation in Gaussian98. Part I. The Calculation of Energies, Gradients, Vibrational Frequencies and Electric Field Derivatives. *J. Mol. Struct.* **1999**, *462*, 1−21.
(56) Stewart, J. J. P. Optimization of Parameters for Semiempirical Methods V: Modification of NDDO Approximations and Application to 70 Elements. *J. Mol. Model.* **2007**, *13*, 1173−1213.
(57) Sheka, E. F.; Shaymardanova, L. K. C_{60}-Based Composites in View of Topochemical Reactions. *J. Mater. Chem.* **2011**, *21*, 17128−17146.
(58) Cox, E. G.; Cruikshank, D. W. J.; Smith, J. A. S. The Crystal Structure of Benzene at −3° C. *Proc. R. Soc. London* **1958**, *A247*, 1−2.
(59) Sinnokrot, M. O.; Valeev, E. F.; Sherrill, C. D. Estimates of the Ab Initio Limit for $\pi-\pi$ Interactions: The Benzene Dimer. *J. Am. Chem. Soc.* **2002**, *124*, 10887−10893.
(60) Zheng, G.; Wang, Z.; Irle, S.; Morokuma, K. Origin of the Linear Relationship between CH_2/NH/O-SWNT Reaction Energies and Sidewall Curvature: Armchair Nanotubes. *J. Am. Chem. Soc.* **2006**, *128*, 15117−15126.
(61) Han, S.; Yoon, M.; Berber, S.; Park, N.; Osawa, E.; Ihm, J.; Tomanek, D. Microscopic Mechanism of Fullerene Fusion. *Phys. Rev. B* **2004**, *70*, 113402.
(62) Matsuzawa, N.; Ata, M.; Dixon, D. A.; Fitzgerald, G. Dimerization of C_{60}: The Formation of Dumbbell-Shaped C_{120}. *J. Phys. Chem.* **1994**, *98*, 2555−2563.
(63) Stepanian, S. G.; Karachevtsev, V. A.; Plokhotnichenko, A. M.; Adamowicz, L.; Rao, A. M. IR Spectra of Photopolymerized C_{60} Films. Experimental and Density Functional Theory Study. *J. Phys. Chem. B* **2006**, *110*, 15769−15775.
(64) Bekyarova, E.; Sarkar, S.; Niyogi, S.; Itkis, M.; Haddon, R. Advances in the Chemical Modification of Epitaxial Graphene. *J. Phys. D: Appl. Phys.* **2012**, *45*, 154009.
(65) Yazyev, O. V.; Louie, S. G. Topological Defects in Graphene: Dislocations and Grain Boundaries. *Phys. Rev. B* **2010**, *81*, 195420.
(66) Elias, D. C.; Nair, R. R.; Mohiuddin, T. M. G.; Morozov, S. V.; Blake, P.; Halsall, M. P.; Ferrari, A. C.; Boukhalov, D. W.; Katsnelson, M. I.; Geim, A. K; et al. Control of Graphene's Properties by Reversible Hydrogenation: Evidence for Graphane. *Science* **2009**, *323*, 610−613.
(67) Schniepp, H. C.; Kudin, K. N.; Li, J.-L.; Prud'homme, R. K.; Car, R.; Saville, D. A.; Aksay, I. A. Bending Properties of Single Functionalized Graphene Sheets Probed by Atomic Force Microscopy. *ACS Nano* **2008**, *2*, 2577−2584.
(68) Zobelli, A.; Ivanovskaya, V.; Wagner, P.; Suarez-Martinez, I.; Yaya, A.; Ewels, C. P. A Comparative Study of Density Functional and Density Functional Tight Binding Calculations of Defects in Graphene. *Phys. Status Solidi B* **2012**, *249*, 276−282.